RSC Advances

PAPER

View Article Online
View Journal | View Issue

Cite this: *RSC Adv.*, 2019, **9**, 4849

Aggregation-induced chiroptical generation and photoinduced switching of achiral azobenzene-*alt*-fluorene copolymer endowed with left- and right-handed helical polysilanes†

Hailing Chen,[a] Lu Yin,[a] Meng Liu,[a] Laibing Wang,[b] Michiya Fujiki, *[b] Wei Zhang *[a] and Xiulin Zhu[ac]

Received 12th November 2018
Accepted 22nd January 2019

DOI: 10.1039/c8ra09345h

rsc.li/rsc-advances

The left and right helicities of azobenzene (Azo)-containing main-chain polymer (PF8Azo) were successfully controlled with an enantiomeric pair of rigid rod-like helical polysilanes carrying (*S*)- and (*R*)-2-methylbutyl groups (PSi-*S* and PSi-*R*, respectively) as their hetero-aggregates in a mixture of chloroform and methanol solvents and in the solid state. Optimizing the good and poor cosolvents and their volume fractions showed that the molar ratio of PF8Azo to PSi-*S*/-*R* and the molecular weight of PF8Azo were crucial to boost the CD amplitudes of PF8Azo/PSi-*S* and PF8Azo/PSi-*R* hetero-aggregates. The photoresponsive *trans*–*cis* transformation caused noticeable changes in the sign and magnitude of the chiroptical behavior due to the hetero-aggregates. Moreover, the optically active PF8Azo homo-aggregates were produced by complete photoscissoring reactions at 313 nm, which could be assigned to the Siσ–Siσ* transitions of PSi-*S* and PSi-*R*.

1 Introduction

Chirality plays key roles in living organisms, medicines, toxins, aromas and flavors (bitter and sweet), immunity, chiroptical functional materials and devices, and the origin of life.[1–6] Generally, several chemical and physical origin biases are applied to efficiently generate and control the chirality of desired materials when achiral starting materials are employed. However, chiral chemical sources are usually well-defined molecules that specifically work toward achiral substances operated at controlled reaction conditions, while chiral physical sources are non-specific and often inefficient.

To obtain more versatile and efficient chiral biases, scientists have investigated several chiral stimuli. For example, two types of chiral lights (circularly polarized light due to angular momentum and vortex light due to orbital angular momentum),[7–15] chiral nematic liquid crystals and chiral terpenes,[16–30] chiral molecules with functional groups,[31,32] hydrodynamic swirling flow,[33,34] and biological and artificial helical polymers[35] induce supramolecular chirality when achiral and optically inactive molecules and polymers are employed. These driving forces are non-covalent intermolecular weak forces including π–π, C–H/π, C–H/O, C–H/F, cation/π, dipole–dipole, and van der Waals (London dispersion) interactions.

Among these strategies, chiral biological and synthetic molecules have been used as helix-inducible scaffolds and templates to construct supramolecular chiral and/or helical architectures from achiral or optically inactive macromolecular sources.

For example, the helical architecture of poly(1-phenylacetylene)-bearing functional groups was inducible in the presence of several chiral amines as scaffolds. This architecture displayed memory effect after removal of the chiral molecules, followed by replacement of achiral amines and amino alcohols.[36,37] Notably, the memory effect is greatly affected by the number of methylene spacers in the achiral molecules. Also, supramolecular chirality of achiral porphyrin derivatives carrying long alkyl chains can be induced during the formation of a co-gel with a glutamate derivative acting as an efficient gelator in DMSO.[38] Liu *et al.* and Ihara *et al.* demonstrated the transfer of molecular chirality to supramolecular gels using a series of chiral amphiphiles derived from L- and D-glutamide.[39–42] Recently, one of the authors (WZ) reported for the first time that two achiral π-conjugated polymers (PSi8 and PCz8) could result in the corresponding helical co-gels with the

[a]*Suzhou Key Laboratory of Macromolecular Design and Precision Synthesis, Jiangsu Key Laboratory of Advanced Functional Polymer Design and Application, State and Local Joint Engineering Laboratory for Novel Functional Polymeric Materials, College of Chemistry, Chemical Engineering and Materials Science, Soochow University, Suzhou Industrial Park, Suzhou 215123, China. E-mail: weizhang@suda.edu.cn*

[b]*Division of Materials Science, Nara Institute of Science and Technology, 8946-5, Takayama, Ikoma, Nara 630-0192, Japan. E-mail: fujikim@ms.naist.jp*

[c]*Global Institute of Software Technology, No. 5 Qingshan Road, Suzhou National Hi-Tech District, Suzhou 215163, China*

† Electronic supplementary information (ESI) available: CD spectra and DLS *etc.* See DOI: 10.1039/c8ra09345h

help of L- and D-glutamide gelators through multiple weak interactions between the long *n*-alkyl chains, and the helicity of PSi8 and PCz8 was also maintained after the removal of the gelators despite the loss of weak interactions.[43]

Furthermore, naturally occurring and artificial chiral/helical compounds (*e.g.*, DNA, polysaccharides, nucleic acids, synthetic polymers, oligopeptides, and carbon nanotubes (CNTs)) can serve as chirality-inducible templates and scaffolds.[44–54] Recently, researchers found that a DNA-based origami supramolecular polymer was an efficient template to dynamically control the superstructure of gold nanorods, as shown by the changes in the chiroptical properties.[55]

Among the naturally occurring chiral/helical compounds, cellulose is the most abundant polysaccharide on earth. Recently, soluble cellulose triacetate (CTA) and cellulose acetate butyrate (CABu) were reported to be efficient scaffolds capable of transferring their chirality and/or helicity to achiral/non-helical semi-flexible non-charged oligo- and poly(dialkylfluorene)s without chiral catalysts.[52–54] This strategy is of particular significance because of the established linkage between chiral biopolymers and artificial achiral/racemic materials.

Recently, one of the authors (MF) reported that non-charged poly(*n*-hexyl-(*S*)-2-methylbutylsiane) (PSi-*S*) and poly(*n*-hexyl-(*R*)-2-methylbutylsiane) (PSi-*R*) function as photoscissorable helical platforms to generate circularly polarized luminescent (CPL)-active and circular dichroism (CD)-active poly(dioctylfluorene) (PF8),[56] poly(dioctyfluorene-*alt*-bis(thiophenyl)benzothiazole) (PF8DBT)[57] and poly(dioctyfluorene-*alt*-bithiophene) (PF8T2)[58] dispersed in a mixture of achiral good and poor solvents. Because of their photoscissorable nature, the CPL and CD activities of the resulting π-conjugated polymers were maintained even after the removal of helical PSis.

To further verify the scaffolding capability of PSi-*R* and PSi-*S*, we chose non-charged, non-helical poly((9,9-dioctylfluorenyl-2,7-diyl)-*alt*-4,4′-azobenzene) (PF8Azo, Fig. 1) as a photoinduced *trans–cis* isomerizable polymer. Azobenzene (Azo) derivatives are commonly used as photoresponsive building blocks, and their reversible photoinduced *trans–cis* isomerization causes significant changes in their physical and chemical properties.[25–30,59] The combination of the chiroptical properties and photoisomerisability efficiently provides reversible chiroptical switching behavior. Herein, we reported unique photoinduced change in CD-active PF8Azo hetero-aggregates endowed with PSi-*S* and PSi-*R* under optimized conditions. The CD amplitudes of the PF8Azo aggregates were maintained even after the photoscissoring of PSi-*S* and PSi-*R* at 313 nm at the Si-Si main chain.

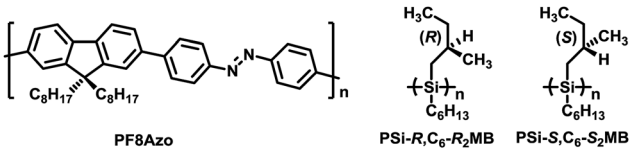

Fig. 1 Chemical structures of PF8Azo (M_n = 23 900 Da, M_w/M_n = 1.61, DP_n = 42), PSi-*R* (M_n = 23 900 Da, M_w/M_n = 1.64, DP_n = 128), PSi-*S* (M_n = 20 400 Da, M_w/M_n = 1.31, DP_n = 110).

2 Experimental section

Materials

Preparation of PSi. The preparation and characterization of PSi-*S* and PSi-*R* used in this work are described in the experimental section of the reference in detail.[56]

Preparation and separation of azo-containing polymers. The preparation and characterization of PF8Azo[26] and PMMAzo[28] are provided in the experimental sections of the references. PF8Azo samples with different molecular weights were separated using a recycling preparative HPLC system.

Hetero-aggregation of azo-containing polymers with PSi-*S*/*R* and preparation of dried aggregates. Spectroscopic-grade chloroform ($CHCl_3$) and tetrahydrofuran (THF) (Dojindo, Kumamoto, Japan) as good solvents and methanol (MeOH), *n*-hexane, ethanol and isopropanol (Dojindo, Kumamoto, Japan) as poor solvents were combined to produce a hetero-aggregate in a synthetic quartz (SQ)-grade cuvette (path length: 10 mm). A series of preliminary results allowed us to optimise a combination of $CHCl_3$ and MeOH to efficiently generate the hetero-aggregate with greater CD amplitudes. The best volume fraction of $CHCl_3$-to-MeOH and the best molar ratio of Azo-polymers-to-PSi-*S*/*R* were tuned according to the experimental requirements. To the cuvette, the dissolved azo-polymers were added, followed by adding first PSi-*S*/*R* solution and finally MeOH to produce well-mixed hetero-aggregates dispersed in a mixture of $CHCl_3$ and MeOH. The total volume of the cosolvents was fixed to be 3.0 mL. Subsequently, CD-UV-vis spectroscopic data were collected immediately in several minutes after generation of the hetero-aggregates. The dried aggregates were prepared by removing the co-solvent by flushing a dry nitrogen gas at room temperature. The dried hetero-aggregate was dispersed in silicone grease (Dow–Corning–Toray). The aggregate-containing grease was smeared onto both sides of a quartz disk (22 mm in diameter).

Characterisation

Chiroptical analysis. The dissymmetry factor of CD in the ground state was calculated using $g_{CD} = (\varepsilon_L - \varepsilon_R)/[(\varepsilon_L + \varepsilon_R)/2]$, where ε_L and ε_R represent the extinction coefficients for left- and right-circularly polarized lights, respectively. The parameter g_{CD} was obtained using the following equation: $\Delta\varepsilon/\varepsilon$ = [ellipticity (in mdeg)/32 980]/absorbance at the CD extremum of the aggregates. The g_{CD} value refers to the degree of circular polarization in the ground state of the aggregates.

Instrumentation

The CD and UV-vis spectra of the solution were obtained simultaneously on a JASCO (Hachioji-Tokyo, Japan) J-815 spectropolarimeter with a Peltier-controlled apparatus to control the sample temperature. A quartz cuvette (SQ-grade) with a 10 mm path length was used. The parameters for obtaining the CD/UV-vis spectra are as follows: scanning rate = 100 nm min^{-1}, bandwidth = 2 nm, response time = 2 seconds, single accumulation and 1 nm interval sampling. The number-average molecular weight (M_n) and polydispersity ($Đ = M_w/M_n$)

of the polymers were characterized by a TOSOH HLC-8320 gel permeation chromatograph (GPC) (Tokyo, Japan) equipped with a refractive index and UV detectors using two TSKgel Super Multipore HZ-N columns (4.6 × 150 mm, 3 μm particle size) enabling molecular weight analysis ranging from 7×10^2 to 2×10^5 g mol^{-1}. THF was used as an eluent at a flow rate of 0.35 mL min^{-1} at 40 °C. These samples were calibrated with polystyrene standards (TOSOH). The recycling preparative HPLC Mode LC-9260NEXT equipped with a manual injector, UV-vis 4ch (200–800 nm) and RI-700NEXT detectors, using JAIGEL-2HH and JAIGEL-2.5HH (PS/DVB packing material) columns, was used to obtain a broad range of molecular weights of PF8Azo. The flow rate of THF is 6 mL min^{-1} at room temperature. Dynamic light scattering (DLS) measurements were performed with a Zetasizer Nano ZS instrument (Malvern, Worcestershire, UK) at room temperature. An ultra-high-pressure 500 W Hg lamp (Optiplex BA-H501 and USH-500SC2, Ushio [Tokyo, Japan]) with three narrow band-pass filters at 313 nm, 405 nm and 546 nm was irradiated to destruct PSi-*S*/-*R* and to photoisomerize the hetero-aggregate as a suspension in a cuvette at room temperature. The irradiation intensity was characterised as 128 μW cm^{-2} at 313 nm, 159 μW cm^{-2} at 405 nm and 589 μW cm^{-2} at 546 nm using a broadband photodetector Ophir Optronics with Nova with photodiode head PD300-UV (Tel-Aviv, Israel).

3 Results and discussion

Emerging CD-active PF8Azo induced by chirality/helicity of PSi-*S* and PSi-*R*

Fig. 2 shows the distinct bisignate CD bands at 305 and 322 nm that are characteristic of an exciton couplet of an Siσ–Siσ* transition arising from the helically assorted aggregates of PSi-*S* and PSi-*R*. However, it should be noted that additional negative/positive CD bands at the corresponding broader UV-vis spectra in the range of 350–550 nm originated from the π–π* transition

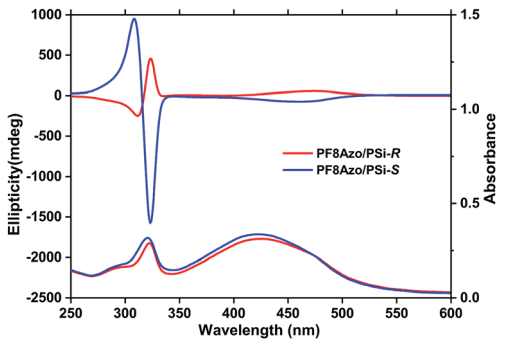

Fig. 2 The CD and UV-vis spectra of PF8Azo/PSi-*S* (blue line) or PF8Azo/PSi-*R* (red line) hetero-aggregates. The hetero-aggregates were present at 1-to-1 molar ratio as repeating units in $CHCl_3$–MeOH (2.0/1.0, (v/v)) cosolvent. The final concentrations of $[PSi\text{-}S/\text{-}R]_0$ and $[PF8Azo]_0$ were 1.0×10^{-5} M and 1.0×10^{-5} M, respectively. The single sign of the broad CD bands in the visible region was assigned to the π–π* transitions of the PF8Azo main chain induced by the chirality/helicity of the rigid rod-like helical PSi-*S* and PSi-*R*.

of the PF8Azo aggregate itself. Meanwhile, the signs of these CD bands were directly related to the chirality/helicity of employed PSi. The g_{CD} values at 475 nm increased to $+9.1 \times 10^{-3}$ for PF8Azo/PSi-*R* and -10.5×10^{-3} for the PF8Azo/PSi-*S* hetero-aggregate. These spectral characteristics of the PSi-PF8Azo hetero-aggregates were nearly consistent with those of chiral light-induced polymer homo-aggregates.[9,10] For comparison, the CD and UV-vis spectra of PF8Azo, PSi-*S* and PSi-*R* homo-aggregates were obtained after dispersion in $CHCl_3$–MeOH (2/1, (v/v)) cosolvent at room temperature; the spectra are shown in the ESI (Fig. S1†). Evidently, PF8Azo homo-aggregates did not reveal a helix preference, while the PSi-*S* and PSi-*R* homo-aggregates exhibited significant bisignate CD band characteristics due to the exciton couplet in the near-UV region.

These comparative measurements indicated that the helicity/chirality of PSi-*S*/-*R* can efficiently transfer to non-charged PF8Azo during hetero-aggregation. Clearly, the chirality/helicity of the hetero-aggregate could be maintained and increased by embedding in silicone grease (Fig. S2, ESI†), as indicated by a comparison of the corresponding g_{CD} values. The g_{CD} values at λ_{ext} (320 nm) of PF8Azo/PSi-*S* and PF8Azo/PSi-*R* hetero-aggregates were -27.6×10^{-3} and $+4.6 \times 10^{-3}$ in the cosolvent, respectively, and -26.4×10^{-3} and $+7.0 \times 10^{-3}$ in the grease, respectively. However, the vinylpolymer containing azo-side-chain (PMMAzo) did not produce the corresponding CD-active PMMAzo during hetero-aggregation with PSi-*S* in any mixtures of $CHCl_3$ and MeOH cosolvents (Fig. S3, ESI†). A plausible explanation is that floppy PMMAzo could not wrap efficiently around the semi-flexible PSi-*S* helical main chains due to inefficient intermolecular interactions. Also, PF8Azo that is a semiflexible π-conjugated polymer efficiently interacted with semi-flexible PSi-*S*. The main rigidity of two polymers was assumed to be crucial.

To further optimize the hetero-aggregation conditions, we determined the best volume fractions of several good and poor solvents associated with the best molar ratio of PF8Azo to PSi-*S*/-*R*.

First, we systematically surveyed $CHCl_3$ and THF as good solvents, while alcoholic solvents (ethanol, MeOH and isopropanol) and *n*-hexane were chosen as poor solvents. A series of CD/UV-vis spectral data sets (Fig. S4, ESI†) showed that the spectral amplitudes of the PF8Azo/PSi-*S* hetero-aggregate are very weak or nearly CD-silent except for the $CHCl_3$–MeOH cosolvent. Alcoholic solvents were preferred over *n*-hexane as poor solvents to efficiently produce the CD-active hetero-aggregates.

Next, we optimized the molar ratios of the repeating units between PF8Azo and PSi-*S*/-*R* in their hetero-aggregates to reach the greatest CD amplitudes in the best volume fraction of the $CHCl_3$ and MeOH (2 : 1) cosolvents. The g_{CD} values as a function of the volume fractions of $CHCl_3$ and MeOH cosolvents are shown in Fig. 3. Also, the g_{CD} values as a function of hetero-aggregates, known as the Job's plot,[60] are given in Fig. 4. The data were taken from the scattering-free CD spectra in Fig. S5 and S6 in the ESI.†

From Fig. 3, we observe that the g_{CD} value of the hetero-aggregates is greatly enhanced at a very specific volume

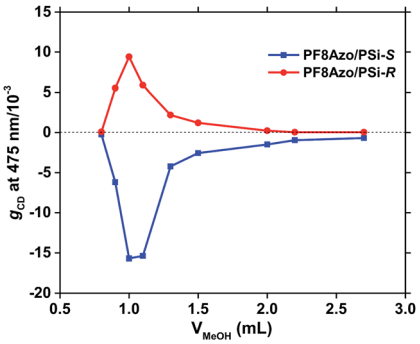

Fig. 3 The g_{CD} values at λ_{ext} of 475 nm of PF8Azo/PSi-*S* (blue) and PF8Azo/PSi-*R* (red) hetero-aggregates as a function of the volume fraction of MeOH (poor solvent) in $CHCl_3$ (good solvent) cosolvents (total volume: 3 mL). The molar ratio was 1 : 1. $[PSi\text{-}S/\text{-}R]_0 = [PF8Azo]_0 = 1.0 \times 10^{-5}$ M in the cuvette.

fraction of $CHCl_3$ (2.0 mL) and MeOH (1.0 mL) when the molar ratio of PSi-*S*/-*R* and PF8Azo is fixed at 1 : 1. This anomaly is ascribed to an optofluidic effect[61] due to photon confinement in a polymeric optical cavity reported in several polymer aggregate systems. Alternatively, the Job's plot in Fig. 4 indicates that the PF8Azo/PSi-*S*/-*R* hetero-aggregates do not obey a sergeant-and-soldier scenario.[62] The g_{CD} values of the hetero-aggregates increased at very specific molar ratios: 1 : 1 for PSi-*S* and PF8Azo and 1 : 2 for PSi-*R* and PF8Azo. The difference in this ratio could be attributed to subtle differences in their M_n and $Đ$ or other unresolved reasons.

Meanwhile, we characterized the hydrodynamic particle sizes of the PSi-*S* and PF8Azo homo-aggregates at different volume fractions of $CHCl_3$–MeOH cosolvents by DLS methods (Tables S1 and S2, ESI†) to monitor the change in the sizes of the homo-aggregates. The particle size of the homo-aggregates gradually decreased as the fraction of $CHCl_3$ increased. A mixture of PSi-*S* and PF8Azo (1 : 1) and a mixture of PSi-*R* and PF8Azo (1 : 1) produced similar sizes (≈700 nm) of hetero-aggregates (Fig. 5). From these results, we concluded that the helicity of the non-helical and non-charged PF8Azo is successfully induced by the helicity/chirality of non-charged PSi-*S*/-*R* during hetero-aggregation in $CHCl_3$–MeOH cosolvents.

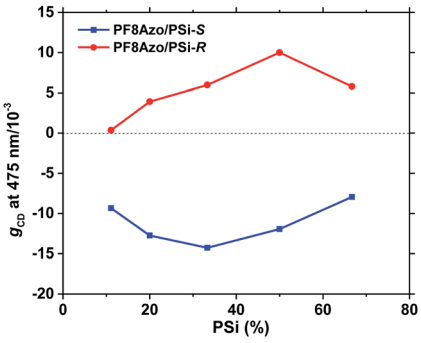

Fig. 4 The g_{CD} value at 475 nm *vs.* the molar ratio of PSi-*S*/-*R* in the PF8Azo/PSi-*S* (blue) and PF8Azo/PSi-*R* (red) hetero-aggregates. $[PF8Azo]_0 = 1.0 \times 10^{-5}$ M. The volume fraction of $CHCl_3$ and MeOH was 2 : 1 (total volume: 3 mL) in all experiments.

Si–Si bond selective photoscissoring reaction of PSi in the PF8Azo/PSi hetero-aggregates

Previous studies have demonstrated the helix scaffolding capability of PSi-*S* and PSi-*R* in the presence of non-charged achiral π-conjugated polymers by rapid photoscissoring of several polysilanes upon near-UV irradiation at the Siσ–Siσ* transition.[56–58,63–65] The result prompted us to further explore the photoscissoring characteristics of rigid helical PSi-*S* and PSi-*R*. The hetero-aggregates of PF8Azo/PSi-*S* and PF8Azo/PSi-*R* exhibited originally intense bisignate (+/−) or (−/+) CD characteristics at ≈320 nm due to the sharper Siσ–Siσ* bands that are parallel to the main chain axis of the Si–Si bond, as seen in Fig. 5(a). Upon irradiation at 313 nm for 10 s, the bisignate CD bands and the corresponding Siσ–Siσ* bands significantly weakened, followed by a distinct red shift (≈10–20 nm) at the

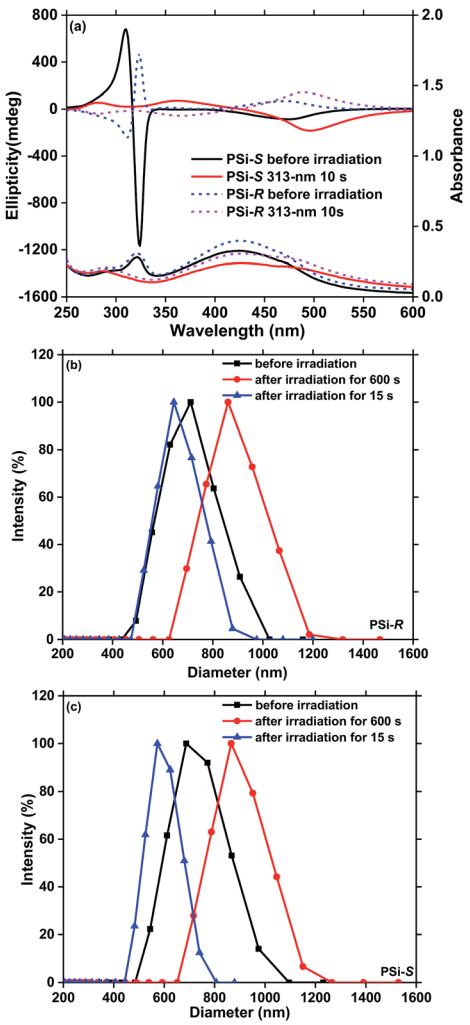

Fig. 5 (a) Changes in the CD and UV-vis spectra of the PF8Azo/PSi-*R* and PF8Azo/PSi-*S* hetero-aggregates before and after the irradiation at 313 nm. Comparisons of hydrodynamic sizes of hetero-aggregates for (b) PF8Azo/PSi-*R* (c) PF8Azo/PSi-*S* before (black line) and after the 313 nm irradiation for 15 s (blue line) and 600 s (red line) obtained *via* DLS. The hetero-aggregates were produced with a volume ratio ($CHCl_3$–MeOH) of 2 : 1 and a molar ratio of 1 : 1 ($[PSi\text{-}S/\text{-}R]_0 = [PF8Azo]_0 = 1.0 \times 10^{-5}$ M).

first Cotton band (≈460 nm) of the PF8Azo aggregate (Fig. 5(a)). These results indicated that PSi-*S* and PSi-*R* decomposed rapidly upon irradiation at 313 nm within 10 s. Enhanced CD signal amplitudes associated with the noticeable red-shift of the PF8Azo/PSi-*S* and PF8Azo/PSi-*R* aggregates suggested a significant structural transition from ill-ordered to well-ordered π–π stacks of PF8Azo by photochemically removing the polysilanes. The origin of the red shift of PF8Azo indicated the production of J-aggregation. Although the near-UV irradiation allowed efficient decomposition of the polysilanes, the chirality of PF8Azo was maintained. The bisignate CD spectral profiles of the PF8Azo aggregates were nearly mirror symmetric (Fig. 5(a)), while the corresponding π–π* CD bands were monosignate spectral profiles for the hetero-aggregates before PSi-*S* and PSi-*R* were photochemically removed (Fig. 2).

Next, we optimized the best irradiation time of the near-UV light source to fully decompose PSi-*S* and PSi-*R* and to avoid undesirable *trans*-to-*cis* transformation of PF8Azo. Sequential alterations in the CD spectral data associated with the aggregate sizes of the PF8Azo/PSi-*S* and PF8Azo/PSi-*R* hetero-aggregates as a function of irradiation time (5 s, 10 s, 15 s and 600 s) of the 313 nm light source are given in Fig. 5(a), S7, S8 and Table S3.† Importantly, PSi-*S* and PSi-*R* decomposed within 5 s. The polysilanes substantially decomposed after 15 s. A prolonged UV-irradiation (600 s) led to definitive decomposition of these polysilanes based on the complete disappearance of the Siσ–Siσ* bands, while the magnitude of the CD-active π–π* bands due to PF8Azo progressively increased and red shifted. These CD/UV-vis spectral alterations at the Siσ–Siσ* and π–π* bands were almost identical to previous results for the non-azobenzene π-conjugated polymers with PSi-*S* and PSi-*R*.[56–58] However, uncharacterized CD-silent species remaining in the solution may afford CD-active PF8Azo.

To characterize the hydrodynamic sizes of the aggregates, we analysed the sizes of the F8Azo/PSi-*R* (Fig. 5(b)) and F8Azo/PSi-*S* (Fig. 5(c)) hetero-aggregates for three irradiation times (0 s, 15 s, and 600 s) of the 313 nm light source by means of the DLS method. Clearly, the original sizes of these hetero-aggregates greatly changed at 15 s and 600 s.

The initial size of the PF8Azo/PSi-*R* hetero-aggregate was ≈650 nm, followed by slight reduction in the size (≈620 nm) after 15 s of UV irradiation. Eventually, the aggregate size increased slightly to ≈810 nm after 600 s of UV irradiation. Similarly, the initial size (≈690 nm) of F8Azo/PSi-*S* hetero-aggregate reduced to ≈580 nm, followed by increase to ≈830 nm after 600 s of 313 nm irradiation. The decreases in the aggregate size were due to the photoscissoring reaction at 313 nm, rapidly breaking the Si–Si bond, followed by dissolution of the resulting fragments with low molecular weights from the aggregates to the surrounding cosolvents. This scenario is similar to a rinsing process with proper solvents when positive-type photoresist materials are employed.

Although these fragments may contribute to smaller aggregates, the increase in the aggregate size is due to the so-called Ostwald ripening,[66] which increases the initial size of the aggregate after the removal of polysilane with the help of the prolonged UV light irradiation and increasing time. By dissolving the smaller aggregates into the solution, the larger aggregates are easy to grow, resulting in apparent increase in the aggregate size.

The Ostwald ripening scenario indicates that (i) smaller particles are easily dissolved into solution but larger particles are not; (ii) smaller particles can deposit onto the surface of larger particles; and (iii) larger particles become much larger, while smaller particles disappear. Actually, in the cases of the homo-aggregates, the hydrodynamic aggregate sizes increased with increasing time (Table S4, ESI†).

Dual wavelength-controlled photoisomerization of PF8Azo in the PF8Azo/PSi hetero-aggregate – all photon-mode chiroptical switching and memory

The advantages of azobenzene-containing polymers, oligomers, and molecules are reversibility and smart functions in photophysical and photochemical properties owing to the *trans–cis* isomerization of the azobenzene framework in response to external photochemical and thermal biases. Previously, we demonstrated thermo-and photoisomerization of the main-chain and side-chain azo-containing polymers in cosolvents. PF8Azo dissolved in $CHCl_3$ showed clear *trans–cis–trans* isomerization capability by applying two different wavelengths of 405 nm and 546 nm (Fig. S9, ESI†). These results prompted us to further investigate the chiroptical switching characteristics of CD-active PF8Azo aggregates as the main-chain type azo polymer was endowed with chirality/helicity of PSi-*S* and PSi-*R*.

Fig. 6 shows the changes in the g_{CD} values at 475 nm of *trans*-PF8Azo/PSi-*R* (red line) and *trans*-PF8Azo/PSi-*S* (blue line) hetero-aggregates in $CHCl_3$–MeOH cosolvent by applying two different wavelengths of 405 nm and 546 nm. Importantly, the 405 nm and 546 nm wavelengths were insensitive to PSi-*S* and PSi-*R* due to the lack of the corresponding transitions in the visible region. For comparison, to obtain the corresponding *cis*-PF8Azo/PSi-*R* and *cis*-PF8Azo/PSi-*S* hetero-aggregates, *cis*-PF8Azo in homogeneous $CHCl_3$ solution was produced by photoirradiation at 405 nm light, followed by hetero-

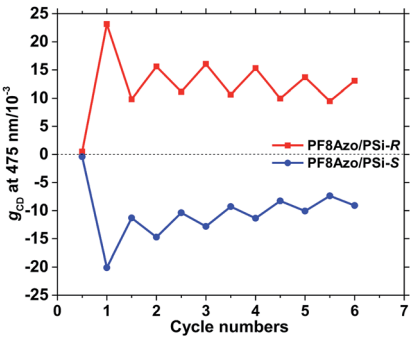

Fig. 6 The g_{CD} values at 475 nm of PF8Azo/PSi-*R* (red line) and PF8Azo/PSi-*S* (blue line) hetero-aggregates upon photoirradiation cycles at 405 nm and 546 nm in $CHCl_3$–MeOH cosolvent (2.0/1.0, (v/v)). Irradiation time: 5 min. ([PSi-*S* or PSi-*R*]$_0$ = [PF8Azo]$_0$ = 1.0 × 10^{-5} M). A $CHCl_3$ solution of PF8Azo was irradiated for 15 min at 405 nm, followed by aggregation with PSi-*S* and PSi-*R* in $CHCl_3$–MeOH cosolvent to obtain the *cis*-PF8Azo/PSi aggregates.

aggregation with PSi-*S* and PSi-*R*. These changes in *cis*- and *trans*-PF8Azo can be recognized by the noticeable changes in the g_{CD} values along with the corresponding CD/UV-vis spectral profiles (Fig. S10, ESI†). These *cis*-PF8Azo/PSi aggregates were initially CD-silent states at the π–π* transition in the visible region. The subsequent 546 nm irradiation for 5 min produced the corresponding *trans*-PF8Azo/PSi hetero-aggregates. Scheme S1† shows the proposed mechanism for this interesting phenomenon, which involves the *cis–trans* photoisomerization of the azobenzene group causing changes in the g_{CD} value.[68,69]

These results allowed us to further investigate the chiroptical switching capability of the CD-active PF8Azo 'homo-aggregate'. The scaffold-induced chiral system can be manifested by the photoresponse results of PF8Azo. By alternating the photo-irradiation of the hetero-aggregate between 405 nm and 546 nm, the *trans*-to-*cis*-to-*trans* isomerization was partly possible because the process is not fully reversible. The reason for this incomplete process is the Ostwald ripening effect during irradiation in the visible region. A modern concept of optofluidics[67] indicates that external and internal lights cannot penetrate large-sized aggregates consisting of π-conjugated chromophores with high absorptivity according to the Lambert–Beer law. Even prolonged photoirradiation did not allow complete *cis–trans* isomerization.

As a comparison, we investigated the chiral side chain effect using two different helical polysilanes to realize the reversibility of photoisomerization. We tested semi-flexible helical polysilane, C_6-S_3MePe (Fig. S11(a), ESI†), in place of rigid helical PSi-*S* (C_6-S_2MB). The side-chain branching of C_6-S_3MePe is located at the γ-position from the Si–Si bond, while that of PSi-*S* (C_6-S_2MB) is located at the β-position. The subtle difference in the branching points definitively determined the main chain flexibility.[63] First, we optimized the volume fraction of the $CHCl_3$–MeOH cosolvents and the molar ratio of PF8Azo-to-C_6-S_3MePe to afford significantly boosted Cotton effect (Fig. S11(b) and (c), ESI†). The optimum conditions for PF8Azo/C_6-S_3MePe were the same as those of PF8Azo/PSi-*S* (C_6-S_2MB) for subsequent photoisomerization studies, but the absolute (+)-sign g_{CD} values around ≈480 nm of PF8Azo greatly decreased.

Owing to C_6-S_3MePe, by alternatively irradiating at 405 nm and 546 nm, the main-chain chirality of PF8Azo around 470 nm of the *cis*-PF8Azo/C_6-S_3MePe hetero-aggregate was reversed compared to that of the *trans*-PF8Azo/PSi-*S* (C_6-S_2MB) hetero-aggregate. A similar *cis–trans* transformation occurred in response to the alternate photoirradiation at 405 nm and 546 nm of the hetero-aggregates (Fig. S11(d), ESI†).

Next, we investigated the concentration dependence of PF8Azo and the molar fraction of PSi-*S* for the PF8Azo/PSi-*S* hetero-aggregate (Fig. S12, ESI†). The photoisomerization capability was similar to the previous conditions mentioned before because a partial *cis–trans* transformation change occurred similarly. However, a PF8Azo sample with a lower molecular weight of 7300 Da ($M_{n,GPC}$) showed a suppressed CD signal associated with the corresponding UV-visible absorption due to PF8Azo that greatly decreased with the irradiation time; the bisignate CD bands due to the Siσ–Siσ* bands were nearly unchanged (Fig. S13, ESI†). The *cis*-PF8Azo aggregate did not undergo any red shift even after 546 nm irradiation. The *cis–trans* photoisomerization of PF8Azo was not significant even upon alternating the irradiation between two wavelengths. Possibly, PF8Azo having lower molecular weight has poor encapsulation capability toward rigid helical PSi-*S*.

Marked M_n effect of CD-active PF8Azo

To know how M_n of PF8Azo affects the CD amplitude of the resulting PF8Azo/PSi hetero-aggregates, indicating the scaffolding capability of PSi-*S* and PSi-*R* to PF8Azo, we investigated the relationship between M_n of PF8Azo and the resulting g_{CD} magnitude of PF8Azo/PSi hetero-aggregates when the M_ns values of PSi-*S* and PSi-*R* were fixed. Fractionated PF8Azo samples were obtained *via* cyclic preparative HPLC. The molar ratios of PF8Azo/PSi-*S* and PF8Azo/PSi-*R* were fixed at 1 : 1. The volume fractions of $CHCl_3$ and MeOH were varied to efficiently enhance the Cotton effect of PF8Azo with different M_n values of the hetero-aggregates. As the value of M_n increased, the solubility of PF8Azo decreased. Thus, the volume fraction of $CHCl_3$ gradually increased to efficiently boost the corresponding CD signal of the hetero-aggregate. Generally, polymers having lower M_n values show better solubility than those having higher M_n values. Nevertheless, from Table S1† and the CD/UV-vis spectra (Fig. S14, ESI†), we consider that the aggregations of PSi-*S* and PSi-*R* were incomplete when the volume fraction of MeOH was less than 23.3%. This condition prevented the efficient generation of PF8Azo hetero-aggregates.

Fig. 7 shows the g_{CD} value at the first Cotton band of the PF8Azo/PSi-*S* and PF8Azo/PSi-*R* hetero-aggregates as a function of M_n of PF8Azo in $CHCl_3$-MeOH cosolvent (2.0/1.0, (v/v)). Clearly, g_{CD} value largely depends on the M_n value. Furthermore, when the value of M_n was greater than 30 000 Da, the hetero-aggregate exhibited small chirality induction capability. PF8Azo with the best M_n value could efficiently interact with PSi-*S* and PSi-*R* at their fixed molecular weights. More detailed M_n and M_W/M_n characteristics of PF8Azo are given in ESI (Table S5†). Thus, the PF8Azo/PSi-S and PF8Azo/PSi-R hetero-aggregates showed enhanced gCD values due to the π–π* transitions when $M_{n,GPC}$ of PF8Azo ranged from 10 000 Da to 20 000 Da. The Da values of PF8Azo corresponding to the DP_n values were 1/4-to-1/5 times that of PSi-*S*/-*R* with fixed M_n.

4 Conclusions

We efficiently induced CD activity at the π–π* transitions of PF8Azo when achiral PF8Azo and rigid rod-like helical PSi-*S* and PSi-*R* were employed as starting materials to produce hetero-aggregates. To efficiently boost the CD signal amplitudes of PF8Azo/PSi-*S* and PF8Azo/PSi-*R* hetero-aggregates, optimizations of the volume fractions of $CHCl_3$ and MeOH as good and poor solvents and the molar ratios of PF8Azo-to-PSi-*S* and PF8Azo-to-PSi-*R* were conducted. By optimizing several parameters, CD-active PF8Azo homo-aggregates were produced by photoscissoring at 313 nm due to the Siσ–Siσ* transition of the PSi-*S* and PSi-*R* main chains. The CD activity of PF8Azo remained unchanged after photoscissoring. The PF8Azo/PSi-*S*

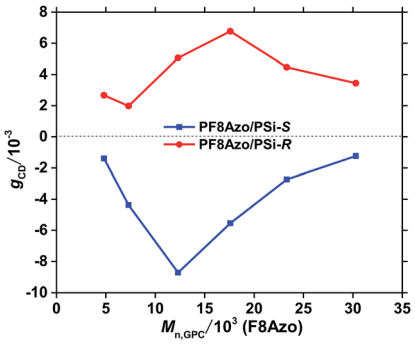

Fig. 7 The g_{CD} values at the first Cotton band of PF8Azo/PSi-*S* and PF8Azo/PSi -*R* hetero-aggregates as a function of M_n of PF8Azo in $CHCl_3$–MeOH cosolvent (2.0/1.0, (v/v)). [PSi-*S* or PSi-*R*]$_0$ = [PF8Azo]$_0$ = 1.0 × 10^{-5} M.

and PF8Azo/PSi-*R* hetero-aggregates underwent *trans–cis* photoisomerization by alternating irradiations at 405 nm and 546 nm.

Conflicts of interest

The authors declare no competing financial interest.

Acknowledgements

The authors are grateful for the financial support from the National Science Foundation of China (21574089), the JSPS KAKEN-HI (16H04155), the Priority Academic Program Development (PAPD) of Jiangsu Higher Education Institutions and the Program of Innovative Research Team of Soochow University.

Notes and references

1 M. Liu, L. Zhang and T. Wang, *Chem. Rev.*, 2015, **115**, 7304–7397.
2 M. A. Mateos-Timoneda, M. Crego-Calama and D. N. Reinhoudt, *Chem. Soc. Rev.*, 2004, **33**, 363–372.
3 E. Yashima, N. Ousaka, D. Taura, K. Shimomura, T. Ikai and K. Maeda, *Chem. Rev.*, 2016, **116**, 13752–13990.
4 M. M. Green, C. Khatri and N. C. Peterson, *J. Am. Chem. Soc.*, 1993, **115**, 4941–4942.
5 E. Yashima, K. Maeda, H. Iida, Y. Furusho and K. Nagai, *Chem. Rev.*, 2009, **109**, 6102–6211.
6 E. Schwartz, S. Le Gac, J. J. L. M. Cornelissen, R. J. M. Nolte and A. E. Rowan, *Chem. Soc. Rev.*, 2010, **39**, 1576–1599.
7 Y. Wang, T. Sakamoto and T. Nakano, *Chem. Commun.*, 2012, **48**, 1871–1873.
8 L. Wang, L. Yin, W. Zhang, X. Zhu and M. Fujiki, *J. Am. Chem. Soc.*, 2017, **139**, 13218–13226.
9 M. Fujiki, K. Yoshida, N. Suzuki, J. Zhang, W. Zhang and X. Zhu, *RSC Adv.*, 2013, **3**, 5213.
10 M. Fujiki, Y. Donguri, Y. Zhao, A. Nakao, N. Suzuki, K. Yoshida and W. Zhang, *Polym. Chem.*, 2015, **6**, 1627–1638.
11 G. Zou, H. Jiang, H. Kohn, T. Manaka and M. Iwamoto, *Chem. Commun.*, 2009, **0**, 5627–5629.
12 T. Kawasaki, M. Sato, S. Ishiguro, T. Saito, Y. Morishita, I. Sato, H. Nishino, Y. Inoue and K. Soai, *J. Am. Chem. Soc.*, 2005, **127**, 3274–3275.
13 M. Watabe, G. Juman, K. Miyamoto and T. Omatsu, *Sci. Rep.*, 2014, **4**, 4281.
14 Y. Taira and M. Katoh, *Astrophys. J.*, 2018, **860**, 45.
15 L. Yin, T. Miao, X. Cheng, Y. Zhao, J. Li, W. Zhang and X. Zhu, *J. Funct. Polym.*, 2018, **5**, 387–401.
16 K. Akagi, G. Piao, S. Kaneko, K. Sakamaki, H. Shirakawa and M. Kyotani, *Science*, 1998, **282**, 1683–1686.
17 H. Goto and K. Akagi, *Angew. Chem., Int. Ed.*, 2005, **44**, 4322–4328.
18 K. Akagi, *Chem. Rev.*, 2009, **109**, 5354–5401.
19 Y. Kawagoe, M. Fujiki and Y. Nakano, *New J. Chem.*, 2010, **34**, 637.
20 Y. Zhao, N. A. Abdul Rahim, Y. Xia, M. Fujiki, B. Song, Z. Zhang, W. Zhang and X. Zhu, *Macromolecules*, 2016, **49**, 3214–3221.
21 Y. Nakano, Y. Liu and M. Fujiki, *Polym. Chem.*, 2010, **1**, 460–469.
22 M. Fujiki, Y. Kawagoe, Y. Nakano and A. Nakao, *Molecules*, 2013, **18**, 7035–7057.
23 J. Liu, J. Zhang, S. Zhang, N. Suzuki, M. Fujiki, L. Wang, L. Li, W. Zhang, N. Zhou and X. Zhu, *Polym. Chem.*, 2014, **5**, 784–791.
24 L. Wang, N. Suzuki, J. Liu, T. Matsuda, N. A. A. Rahim, W. Zhang, M. Fujiki, Z. Zhang, N. Zhou and X. Zhu, *Polym. Chem.*, 2014, **5**, 5920–5927.
25 L. Yin, Y. Zhao, S. Jiang, L. Wang, Z. Zhang, J. Zhu, W. Zhang and X. Zhu, *Polym. Chem.*, 2015, **6**, 7045–7052.
26 W. Zhang, K. Yoshida, M. Fujiki and X. Zhu, *Macromolecules*, 2011, **44**, 5105–5111.
27 S. Jiang, Y. Zhao, L. Wang, L. Yin, Z. Zhang, J. Zhu, W. Zhang and X. Zhu, *Polym. Chem.*, 2015, **6**, 4230–4239.
28 L. Yin, Y. Zhao, M. Liu, N. Zhou, W. Zhang and X. Zhu, *Polym. Chem.*, 2017, **8**, 1906–1913.
29 L. Yin, M. Liu, Y. Zhao, S. Zhang, W. Zhang, Z. Zhang and X. Zhu, *Polym. Chem.*, 2018, **9**, 769–776.
30 T. Miao, L. Yin, X. Cheng, Y. Zhao, W. Hou, W. Zhang and X. Zhu, *Polymers*, 2018, **10**, 612.
31 K. Maeda, M. Ishikawa and E. Yashima, *J. Am. Chem. Soc.*, 2004, **126**, 15161–15166.
32 H. Nakashima, J. R. Koe, K. Torimitsu and M. Fujiki, *J. Am. Chem. Soc.*, 2001, **123**, 4847–4848.
33 E. Ohta, H. Sato, S. Ando, A. Kosaka, T. Fukushima, D. Hashizume, M. Yamasaki, K. Hasegawa, A. Muraoka, H. Ushiyama, K. Yamashita and T. Aida, *Nat. Chem.*, 2010, **3**, 68.
34 K. Okano, M. Taguchi, M. Fujiki and T. Yamashita, *Angew. Chem., Int. Ed.*, 2011, **50**, 12474–12477.
35 L. Zhang and M. Liu, *J. Phys. Chem. B*, 2009, **113**, 14015–14020.
36 E. Yashima, T. Matsushima and Y. Okamoto, *J. Am. Chem. Soc.*, 1997, **119**, 6345–6359.

37 E. Yashima, K. Maeda and Y. Okamoto, *Nature*, 1999, **399**, 449–451.
38 Y. Li, T. Wang and M. Liu, *Soft Matter*, 2007, **3**, 1312.
39 P. Duan, X. Zhu and M. Liu, *Chem. Commun.*, 2011, **47**, 5569–5571.
40 P. Duan, Y. Li, L. Li, J. Deng and M. Liu, *J. Phys. Chem. B*, 2011, **115**, 3322–3329.
41 Q. Jin, L. Zhang and M. Liu, *Chem.–Eur. J.*, 2013, **19**, 9234–9241.
42 H. Jintoku, T. Sagawa, T. Sawada, M. Takafuji, H. Hachisako and H. Ihara, *Tetrahedron Lett.*, 2008, **49**, 3987–3990.
43 D. Yang, Y. Zhao, K. Lv, X. Wang, W. Zhang, L. Zhang and M. Liu, *Soft Matter*, 2016, **12**, 1170–1175.
44 S. Le Gac, E. Schwartz, M. Koepf, J. J. L. M. Cornelissen, A. E. Rowan and R. J. M. Nolte, *Chem.–Eur. J.*, 2010, **16**, 6176–6186.
45 J. D. Le, Y. Pinto, N. C. Seeman, K. Musier-Forsyth, T. A. Taton and R. A. Kiehl, *Nano Lett.*, 2004, **4**, 2343–2347.
46 Y. Guo, H. Oike and T. Aida, *J. Am. Chem. Soc.*, 2004, **126**, 716–717.
47 G. Fukuhara, K. Iida, Y. Kawanami, H. Tanaka, T. Mori and Y. Inoue, *J. Am. Chem. Soc.*, 2015, **137**, 15007–15014.
48 S. Haraguchi, M. Numata, C. Li, Y. Nakano, M. Fujiki and S. Shinkai, *Chem. Lett.*, 2009, **38**, 254–255.
49 T. Shiraki, A. Dawn, Y. Tsuchiya and S. Shinkai, *J. Am. Chem. Soc.*, 2010, **132**, 13928–13935.
50 S. Haraguchi, T. Hasegawa, M. Numata, M. Fujiki, K. Uezu, K. Sakurai and S. Shinkai, *Org. Lett.*, 2005, **7**, 5605–5608.
51 M. Ikeda, T. Hasegawa, M. Numata, K. Sugikawa, K. Sakurai, M. Fujiki and S. Shinkai, *J. Am. Chem. Soc.*, 2007, **129**, 3979–3988.
52 S. Guo, N. Suzuki and M. Fujiki, *Macromolecules*, 2017, **50**, 1778–1789.
53 S. Guo, H. Kamite, N. Suzuki, L. Wang, A. Ohkubo and M. Fujiki, *Biomacromolecules*, 2018, **19**, 449–459.
54 T. Shiraki, Y. Tsuchiya, T. Noguchi, S. Tamaru, N. Suzuki, M. Taguchi, M. Fujiki and S. Shinkai, *Chem.–Asian J.*, 2014, **9**, 218–222.
55 X. Lan, T. Liu, Z. Wang, A. O. Govorov, H. Yan and Y. Liu, *J. Am. Chem. Soc.*, 2018, **140**, 11763–11770.
56 N. A. A. Rahim and M. Fujiki, *Polym. Chem.*, 2016, **7**, 4618–4629.
57 M. Fujiki and S. Yoshimoto, *Mater. Chem. Front.*, 2017, **1**, 1773–1785.
58 S. T. Duong and M. Fujiki, *Polym. Chem.*, 2017, **8**, 4673–4679.
59 A. Natansohn and P. Rochon, *Chem. Rev.*, 2002, **102**, 4139–4175.
60 A. Munoz and A. Virgili, *Tetrahedron: Asymmetry*, 2002, **13**, 1529–1534.
61 P. Domachuk, F. G. Omenetto, B. J. Eggleton and M. Cronin-Golomb, *J. Opt. A: Pure Appl. Opt.*, 2007, **9**, S129–S133.
62 M. M. Green, M. P. Reidy, R. J. Johnson, G. Darling, D. J. Oleary and G. Willson, *J. Am. Chem. Soc.*, 1989, **111**, 6452–6454.
63 M. Fujiki, J. R. Koe, K. Terao, T. Sato, A. Teramoto and J. Watanabe, *Polym. J.*, 2003, **35**, 297–344.
64 R. D. Miller and J. Michl, *Chem. Rev.*, 1989, **89**, 1359–1410.
65 A. Saxena, K. Okoshi, M. Fujiki, M. Naito, G. Guo, T. Hagihara and M. Ishikawa, *Macromolecules*, 2004, **37**, 367–370.
66 P. W. Voorhees, *J. Stat. Phys.*, 1985, **38**, 231–252.
67 C. Monat, P. Domachuk and B. J. Eggleton, *Nat. Photonics*, 2007, **1**, 106–114.
68 A. Bobrovsky, V. Shibaev, A. Bubnov, V. Hamplová, M. Kašpar and M. Glogarová, *Macromolecules*, 2013, **46**, 4276–4284.
69 H. Sogawa, M. Shiotsuki and F. Sanda, *Macromolecules*, 2013, **46**, 4378–4387.